Determination of Electric Field at Inception Based upon Current-Voltage Characteristics of AC Corona in Rod-Plane Gaps

H. Javadi*, M. Farzaneh** and A. Peyda**

Abstract: This paper deals with the measurement of AC corona inception voltage, V_{incp}, at the tip of a rod electrode using a hemispherically-capped rod-plane electrode configuration for various rod radii with a short air gap. Effects of atmospheric pressure and temperature variation on V_{incp} are investigated experimentally. An empirical equation for the field form factors of the hemispherically capped rod-plane electrodes is proposed with its range of applicability. The obtained results are analyzed to derive a more accurate analytical equation for the calculation of the electric field at corona inception voltage, E_{incp}, and the average of electric field distribution, E_{mean}.

Keywords: Electric field, Corona Inception Voltage, Rod-plane Electrodes, Form Factor, Atmospheric Correction Factor, 3-D Electric Field Simulation.

1 Introduction

MANY investigations have been carried out to observe and understand the complex processes underlying breakdown across air gaps. These studies include: (i) the physical process of corona and breakdown across air gaps; (ii) the electric field calculation for various electrode configurations; and (iii) the effect of atmospheric parameters.

Studies in the first category aim at understanding the phenomena and providing explanations of the microscopic interactions involved (electron attachments, photo ionization, velocity of charged particles,…), as well as their manifestations in partial and various arc forms and avalanches, and the relation of discharge current to the different contributing voltages [1-6]. In most of these studies, dc or impulse voltage was used for medium to long air gaps. Although this research provides a good insight into the physics of the breakdown process, it barely has pointed to any clear computation technique or proposed adequate equations for the electric field at the corona inception voltage, E_{incp}.

For the second category of investigations, about electric field calculation for various electrode configurations, most of the literature deals with the numerical computation of electric fields using computer modeling such as the Finite Element Method "FEM" [7] and the Charge Simulation Method "CSM" [8-9] which, though unable to derive analytical formulae, provide close computer simulation. Also, it includes an expression derived for short air gaps in a rod-plane configuration with SF6 insulating medium [10]. However, all these methods provide results which are not validated with laboratory tests for different voltage wave shapes.

There are also a few useful empirical formulae for other highly non-uniform electrode configurations [11-12], but there is no equation for the calculation of E_{incp} at the tip of the rod in a rod-plane electrode system. The only known equation for that purpose was derived by Coelho [13] using a hyperbolic approximation, and has been used in a variety of applications [14-17]. As it is known from the extensive research on the breakdown process, there are different stages of the development of streamers and partial discharges, each depending on a different set of factors and degrees of contribution to the evolving non-uniformity from inception of streamer corona to complete breakdown. It is almost impossible to explain the breakdown process generally for a vast range of rod-plane gaps, because the streamer build-up process varies among a set of gap and rod radius sizes.

Iranian Journal of Electrical & Electronic Engineering, 2010.
Paper first received 23 Aug. 2009 and in revised form 26 May 2010.
*The Author is currently with the Department of Electrical Engineering, Power and Water University of Technology (PWUT), Tehran, Iran
E-mail: javadi@pwut.ac.ir
** The Authors are with the NSERC/Hydro-Quebec/UQAC Industrial Chair on Atmospheric Icing of Power Network Equipment (CIGELE) and Canada Research Chair on Engineering of Power Network Atmospheric Icing (INGIVRE), Université du Québec à Chicoutimi, Chicoutimi, Qc, Canada, G7H 2B1 (www.cigele.ca).

Therefore, one should not assume that this equation is adequate for all rod-gap size ranges. However, some empirical expressions were derived to calculate field form factors in order to estimate the values of the ratio E_{max}/E_{mean} [18-19] for practical purposes in the case of a rod-plane electrode system. The main issue here is that the average value of the electric field distribution, E_{mean}, cannot be adopted universally as it depends on electrode geometry and on the wave shape of the applied voltage.

In the third category of investigations, dealing with the effects of atmospheric parameter variations on the breakdown voltage of rod-plane gaps [21-22], all the studies have shown that the IEC correction method [23-25] has many setbacks and cannot be generally applied to all electrode configurations and voltage wave shapes. Just a few investigations have been carried out on the effect of humidity for a 20 cm air gap, showing that there is a large difference between the threshold and stability fields for smaller air gaps.

The setback arises from the fact that the effect of air density seems to be dependent on the combination of air pressure and temperature, suggesting that the only feasible way to perform tests is to keep one parameter constant while varying the other. Furthermore, previous studies have shown the necessity of further research on the effect of temperature and pressure variation to determine their interaction on AC corona inception voltage, V_{incp}..

2 Experimental Facilities

Fig. 1 shows the schematic diagram of the experimental setup. The high voltage ac transformer of the setup provides the necessary power and voltage to the circuit [26, 27]. The voltage is regulated by a control unit connected to a stabilizing capacitor C_R. The circuit consists of a current limiting resistor, R_d, and a resistive voltage divider comprises two series resistors, R_{m1} and R_{m2}, where these resistors act respectively as the HV arm of the voltage divider and the LV resistor of the measuring arm.

A custom-built interconnecting bushing connects the high voltage circuit to the test chamber through the Faraday cage. The plane electrode is attached to the common ground wire and to the leakage current sensing resistance R_c. The voltage and current signals are fed to a data acquisition system through a voltage conditioner/limiter. The voltage limiter's cut threshold is ±10V (peak).The sampling rate is set to 800 samples with a 4000Hz clock rate. The data is measured and stored using the LABVIEW® software.

To keep the corona inception voltage measurement as high as accurate as possible, humidity, air temperature and air pressure were kept nearly constant for each set of tests. In order to ensure precision of the test results, a standard system (sphere-sphere electrode configuration, Fig. 2) was used to measure the breakdown voltage at the start of each test set. This value was subsequently used to convert the obtained corona inception voltages for that particular test to standard values.

Fig. 3 shows the set of rod electrodes used in the test object. With the available facilities, rod electrodes of radii have been produced by an acceptable level of accuracy. The radii of the rod electrodes were ranged between 0.25 mm and 3.04 mm, with gap spacing ranging from 1 cm to 15 cm in a 1-cm step increment. In other words, this standard geometry delivers a good reference point for converting the obtained values to the standard atmospheric conditions (T=20ºC, P=101.3kPa and h=11g/m^3).

The peak value of applied voltage at the standard conditions is 31.8kV for the specific electrode system used, thus yielding an electric field of 31.8kVcm^{-1}, which is the minimum required to start corona discharge under the test conditions.

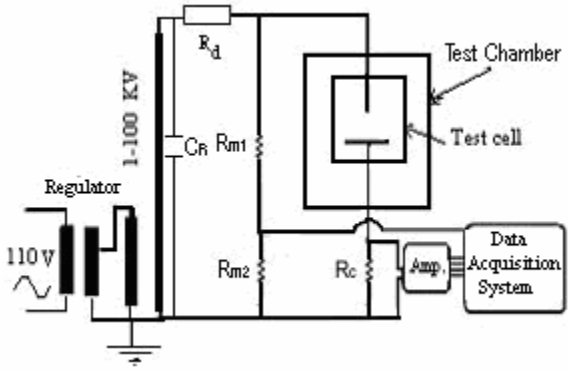

Fig. 1 Circuit diagram of testing setup.

Fig. 2 Standard sphere-sphere electrode.

Fig. 3 Hemispherically-capped steel rod electrodes and test object.

Considering the statistical nature of breakdown, in each case, V_{incp} was measured five times and the mean value was recorded. V_{incp} is easily detectable because of the appearance of partial discharge, and the deformation of the current wave shape including a phase shift from 90 to 0degree (pure capacitive current towards pure resistive one). In order to measure the corona inception voltage, three traditional methods were evaluated.

1. Audio detection
2. Visual detection
3. Current wave shape

So, the analysis of current wave shapes was found to be the best way to measure the corona inception voltage. Current and voltage were simultaneously recorded with a voltage rise rate of 5kV/sec. Since partial discharges appear differently on the current waveforms for different radii and electrode gap distances, these recordings were thoroughly studied to figure out a suitable protocol for corona inception detection by discharge current waveform.

The maximum variations of the atmospheric parameters have been recorded for each set of tests, and were found to be:

1. Ambient temperature: 4°C
2. Atmospheric pressure: 0.005b
3. Humidity: 8 %=1.56gr/m^3 (this humidity change occurred between two extreme values of 7.7 and 9.24gr/m^3)

It should be noted that these maximum variations did not occur during the same test sets and did not cause any error in the results.

3 Experimental Results

The results of the laboratory tests are subdivided into three categories. In the first category, we find the measured values of corona inception voltage for the purpose of deriving an equation to calculate E_{incp} and E_{mean} at the tip of the rod. The second category comprises the data obtained from atmospheric pressure tests. In the third category the last measured values of corona inception voltage under temperature variation are found.

3.1 Measured V_{incp} using the Rod-Plane Electrode Configuration

Considering the unit procedure for the whole geometry range ($0.25mm\langle r\langle 3.04mm$ and $1cm\langle d\langle 15cm$), leakage current and voltage across the gap were recorded using the LabView software. Since peculiar current wave shape deformities are associated with different gap geometries, all the waveforms were meticulously analyzed and studied to detect the point of corona inception.

Fig. 4 shows the detection point of corona inception voltage in a rod-plane electrode configuration with r=2.48mm and d=4cm. Generally, this point is characterized by a slight degree of deformity, an envelope of partial discharges appearing as noise on the gap leakage current waveform and departure of current phase from 90 to 0 degree.

During the laboratory tests, the corona inception regions were observed. From the experimental results, the following categories of corona inception have been distinguished:

- For large-diameter rod tips, no corona was observed during the whole breakdown phenomena. Instead, the initial ionization process manifested itself in the form of disruptive streamer formations. One of the main reasons for that is that the corona critical length is longer than the gap spacing.
- For 0.5mm<r<2.58mm values and for the whole range of gap spacing, a streamer corona developed at an early stage, with a corona film appearing at a later stage.
- For 0.25mm<r<0.5mm and 1cm<d<4cm values, there was a very fast transition period from corona to leader development.
- For 0.25mm<r<1mm and 5cm<d<10cm values, there was a clear and visible presence of corona film on the tip of the rod during a noticeable period.

Fig. 5 also shows a plot of the measured V_{incp} for the whole range of radii 0.25mm<r<3.04mm. As can be noticed, the plot tends to follow a saturation curve pattern.

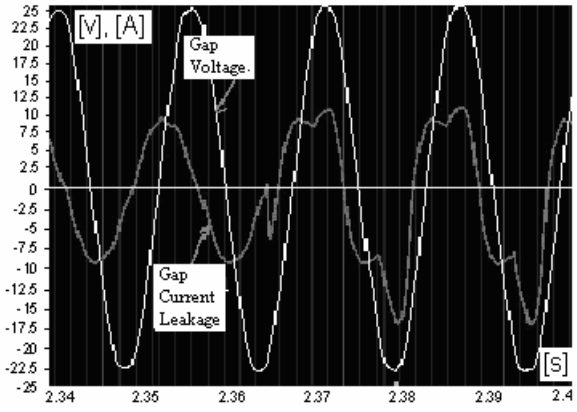

Fig. 4 Corona inception voltage and current wave shape for a rod-plane gap with r=2.48mm and d=4cm.

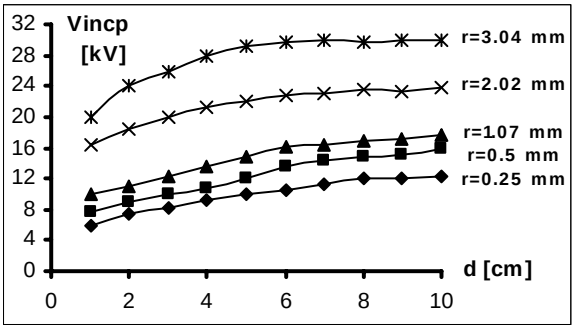

Fig. 5 Corona inception voltage of the rod-plane gaps vs. gap spacing.

3.2 Atmospheric Temperatures Tests

Using a climatic chamber, V_{incp} was measured for a temperature range of -20ºC <T_{amb} <20ºC. The results are plotted in Fig. 6, where the measured values are depicted as circles, and where the dotted line represents the result of a linear regression on these values representing their power trend line. The geometry for these atmospheric tests was set to r=1.54mm with a gap of d=7cm, which approximately represents the mean value of the experimental setup geometry. The plot reveals that a temperature decrease from room temperature to -20ºC has a relatively slight effect on V_{incp}. Over that 40-degree range, V_{incp} increases by about 3.4kV. The test data for the temperature tests are displayed in Table 1. During the tests, the monitored parameters were pressure, temperature, dew point (DP) and relative humidity (RH).

3.3 Atmospheric Pressure Tests

The measured V_{incp} for an ambient pressure, P_{amb}, ranging from 22.8kPa to 101.8kPa, which roughly corresponds to an altitude ranging from 10,500m to 30m, is plotted in Fig. 7, where the circles represent the measured values and where the dotted line is a power curve, fitted to these. This plot shows the fact that air pressure variation affects corona inception voltage more significantly that variation in ambient temperature. For the given pressure range, V_{incp} decreases as low as 9kV at 22.8kPa, which is a considerable drop as compared to that of 21.2kV at 101.8kPa (the altitude of the laboratory in Chicoutimi is roughly 30m above sea level). The chosen geometry for the atmospheric tests is the same as that used for the ambient temperature tests.

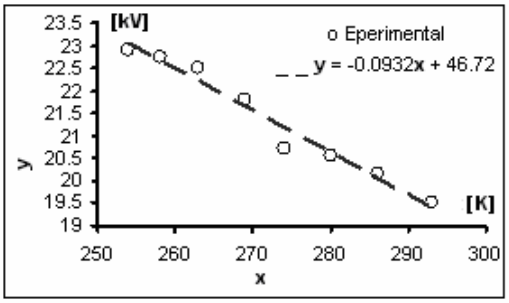

Fig. 6 Effect of decrease in ambient temperature on corona inception voltage for a rod-plane configuration with r=1.54mm and d=7cm.

Table 1 Monitored ambient parameters during the temperature tests.

Air Pressure=101.07 kPa							
Air Temperature ºC							
ºC	**20**	**13.7**	**6.8**	**0.4**	**-10**	**-15**	**-19.4**
V_{incp} (kV)	19.5	20.1	20.6	20.7	22.5	22.8	22.9
h(gr/m^3)	4.1	3	2.2	1.6	0.6	0.3	0.3
RH (%)	24	25.4	29.5	32.9	37	43.6	53
DP (ºC)	-1.3	-5.9	-10.1	-14.7	-23.5	-24.7	-26.3

Table 2 provides the monitored ambient parameters during the tests.

4 Computer Simulation

Since electric field is not measurable experimentally, computer simulation is needed to determine E_{max} and the form factor of each rod-plane electrode.

This simulation was carried out using the Finite Element Method (FEM) based on the Coulomb-3D software for solving static field problems in a three dimensional medium.

4.1 Modeling of Rod-Plane Gaps

For the purpose of computer modeling, exact replicas of the physical configurations were used. The all boundaries of study area were considered the Neumann's type except at the rod electrode (as high voltage electrode using 1V in per unit value) and at the plane electrode (as ground electrode using 0V) considered as Dirichlet's type. Fig. 8 depicts a 3-D model for a rod-plane gap with r=1.54mm and d=4cm, used for atmospheric temperature and pressure tests. Fig. 9 illustrates the distribution of electric strength on a profile plane perpendicular to the y-axis for the same gap arrangement. In that figure, the magnitude of the electric strength is represented by color shades. As expected, the maximum field strength, E_{max}, in the air gap is located at the tip of the rod, right on the central longitudinal axis of the rod.

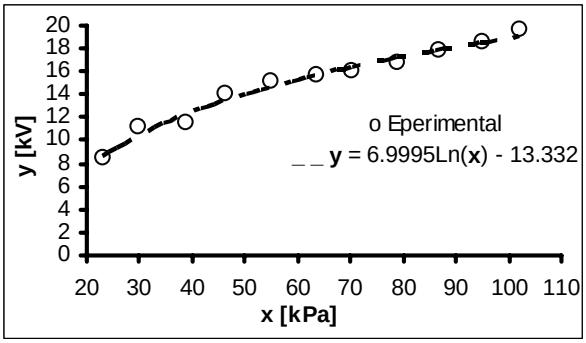

Fig. 7 Effect of ambient pressure reduction on the corona inception voltage for a rod-plane arrangement with r=1.54mm and d=7cm.

Table 2 Monitored ambient parameters during the pressure tests.

Air Temperature=21ºC							
Air Pressure kPa							
kPa	101.8	94.8	86.8	78.8	54.8	38.8	22.8
V_{incp} (kV)	19.5	18.5	17.8	16.7	15	11.5	8.3
h(gr/m^3)	3.42	3.24	3.2	3.06	2.53	2.1	1.9
RH (%)	18.3	17.2	17.2	16.6	14.7	12.6	11.6
DP (ºC)	-3.7	-4.4	-4.6	-5.2	-6.8	-8.9	22.8

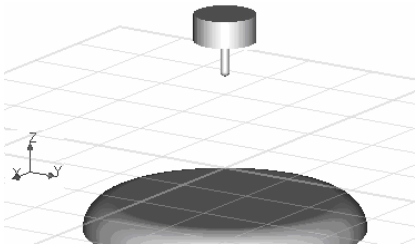

Fig. 8 3-D model of a rod-plane gap of r=1.54mm and d=4cm.

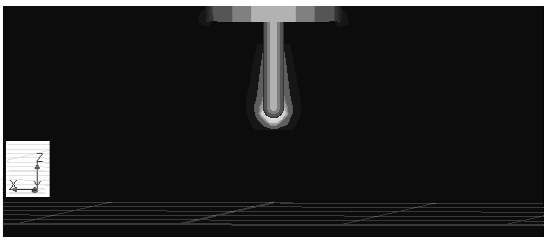

Fig. 9 Distribution of electric field in the gap area for an arrangement with r=1.54mm and d=4cm.

4.2. Analytic and Simulation Results

Coelho et al. proposed an equation based on a simple hyperboloid geometric approximation to calculate the electric field in a point-plane gap. A tip can be generated by the hyperbola of Eq. (1) rotating around the x axis shown in Fig. 10.

$$x = a\sin\xi\cosh\eta$$
$$y = a\cos\xi\sinh\eta \qquad (1)$$

where ζ is the parameter defining the hyperbola. If ζ=0, it corresponds to the Oy axis generating plane. If ζ=π/2, (y=0), it corresponds to the Ox axis generating an infinitely sharp hyperbola. η is the parameter defining a particular point on the hyperbola defined by ζ. The value of the electric field at point (ζ, η) is given by Eq. (2):

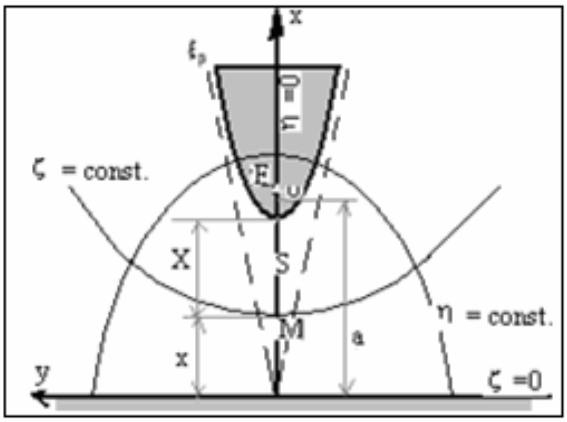

Fig. 10 Representation of a point-plane configuration with the various quantities involved.

$$E(\zeta,\eta) = \frac{C}{a\cos\zeta(\cosh^2\eta - \sin^2\zeta)^{\frac{1}{2}}} \qquad (2)$$

where C is a constant depending on the applied voltage. If we set η=0, the above equation then represents the field along the x axis. In this particular case, making use of some approximations, at the tip (X=0), Eq. (3) is obtained:

$$E(0) = \frac{C}{r} = \frac{V}{r\ln\left(2\left(\frac{a}{r}\right)^{\frac{1}{2}}\right)} \qquad (3)$$

Assuming that $d \approx a$ in Eq. (3), the electric field strength at the tip of the rod can be analytically obtained using Eq. (4).

$$E_{incp} = \frac{2V}{r\ln\left(\frac{4d}{r}\right)} \qquad (4)$$

where V is the applied voltage, r is the rod radius, and d is the gap length.

In Fig. 11, the simulation results and the values obtained by *Coelho*'s equation are compared. Both plots represent E_{max} at the tip of the rod for a gap distance of 1cm<d<10cm for 1cm increments, and a distance of 15cm in the case of an applied voltage of 1 V on the rod electrode.

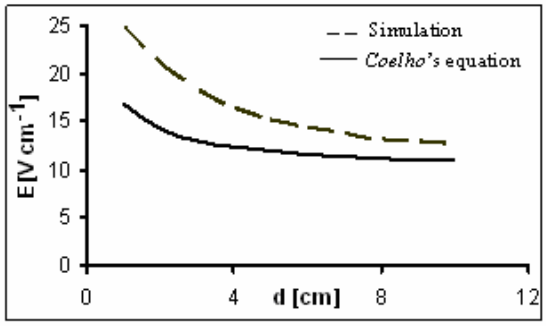

(a)

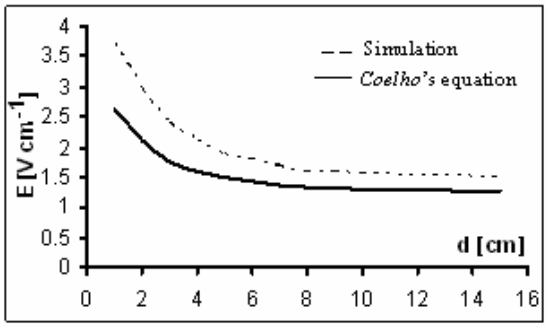

(b)

Fig. 11 Electric field at the tip of the rods vs. gaps for an applied voltage of 1 V on the rod. (a) r=0.25mm (b) r=3.04mm

It is obvious from these plots that:

- The smaller the radius of the rod and the shorter the gap, the higher is the error associated with *Coelho*'s equation.
- The maximum error of *Coelho*'s equation occurs at r=0.25mm and d=1cm with the value of 9 Vcm^{-1}. The minimum error occurs at r=3.04mm and d=15cm with the value of 0.25Vcm^{-1}.
- *Coelho*'s equation provides fairly good results for r>1.54mm and d >10cm.

5 Equation and Data Analysis

The test and simulation results were used to derive equations to calculate f, E_{mean} and E_{incp} for the prescribed ranges of the rod-plane electrode arrangements. Moreover, correction factors for standard atmospheric conditions for air pressure and temperatures were also derived from the experimental results.

5.1 Field form Factor Expression

Using the values of E_{max} and E_{mean} following the computer simulations, the field form factors were calculated by means of Eq. 5,

$$f = \frac{1}{\gamma} = \frac{E_{\max}}{E_{mean}} \tag{5}$$

where E_{mean} is simply the ratio of the corona inception voltage of a rod-plane gap to the gap spacing The results are demonstrated in Fig. 12.

Then, using Matlab's curve fitting tool package, the best fit was applied to the obtained data to achieve an analytic relation. Equation 6 is derived from the data obtained by simulation in order to calculate form factors for the prescribed gap to radius range.

$$f = n.e^{\left(j\frac{d}{r}\right)} + s.e^{\left(l\frac{d}{r}\right)} \quad \text{for} \quad 3 \le \frac{d}{r} \le 400 \tag{6}$$

where n=60.79, j=0.002, s=-58.1, and l=-0.006.

5.2 Expression for Calculating Mean Electric Strength

Normally for an electrode configuration, typically a parallel plane configuration, the point of breakdown and corona discharge inception voltages are the same, i.e around 31 kVcm^{-1} in the air. Nevertheless, in the case of configuration producing highly non-uniform electric fields around their gap, this value varies considerably. Some factors affect that value are atmospheric conditions, electrode shape and arrangement and applied voltage waveform.

It would be very useful for researchers or engineers to have at their disposal an expression to calculate the mean electric strength in a rod-plane air gap at the point of the corona/PD inception (AC voltage), thus avoiding the use of expensive test equipment and time-consuming computer simulation.

In order to derive such an expression, after plotting the V_{incp} values obtained by laboratory tests against the gap spacing, regression analysis was applied to obtain the best fit trend line for all the plots, yielding Eq. (7):

$$E_{mean} = Ad^{B} \tag{7}$$

where coefficients A and B are fitting constants for each trend line, and d is the gap spacing.

The second step is to plot the constants, A and B, against the radii, with a resulting linear regression for A and a logarithmic one for B against r, as shown in Eq. (8).

$$A = k_1.r + k_2 \quad \text{and} \quad B = k_3.\ln(r) + k_4 \tag{8}$$

where k_1 to k_4 are known coefficients. By substituting the A and B values from Eq. (8) into Eq. (7), we obtain:

$$E_{mean} = \frac{4.3103 \times r + 5.8558}{d^{(0.021\ln(r)+0.781)}} \tag{9}$$

In this equation, E_{mean} is in kVcm^{-1}, r in mm and d in cm.

Fig. 13 shows the plots of Eq. (9) against gap spacing for two different rod radii. It also compares the values obtained by that equation with experimental ones.

Table 3 also shows the maximum and minimum deviations of the derived equation from the experimental values in percentage as defined in Eq. (10).

$$Dev = \left| \left(\frac{E_{mean(eqn.)} - E_{mean(\exp.)}}{E_{mean(\exp.)}} \right) \times 100 \right| \tag{10}$$

5.3 Calculation of E_{incp}

The corona onset field strength at the tip of the rod can be calculated from a combination of experimental and computer simulation results. This is achieved by Eq. (11).

$$E_{incp} = E_{mean} \times f = \frac{V_{incp} \times f}{d} \tag{11}$$

where E_{incp} is in kVcm^{-1}, E_{mean} is in kVcm^{-1} and f will be dimensionless.

For that purpose, the same procedure to derive E_{mean} is used to calculate the maximum electric strength at the tip of the rod at the corona inception point, yielding Eq. (12):

$$E_{incp} = \frac{89.576}{d^{(0.035\ln(r)+0.091)} \times r^{0.365}} \tag{12}$$

For $0.25mm \le r \le 3.04mm$ and $1cm \le d \le 15cm$

where E_{incp} is in kVcm^{-1}, r is the rod radius in mm and d is the gap length in cm. Table 4 shows maximum and minimum deviations of the values obtained by Eq. (12) from the experimental results.

Also in order to verify Eq. (12), Fig. 14 and Fig. 15 show respectively the results obtained from that equation and those from the hyperboloid method (Eq. 4).

Table 3 Deviation of Eq. (9) from the Experimental Values in Percentage.

Maximum & Minimum deviations (%)			
	Rod Radius (mm)	Gap (cm)	Deviation
Max	1.07	15	14.09%
Min	3.04	8	0.02%

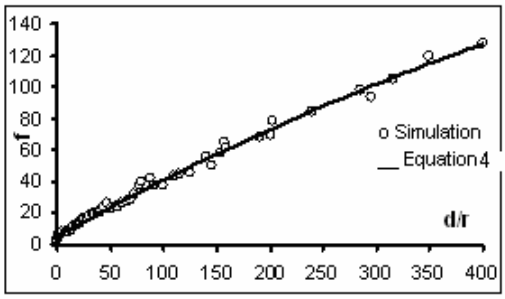

Fig. 12 Form factor value as the function of d/r.

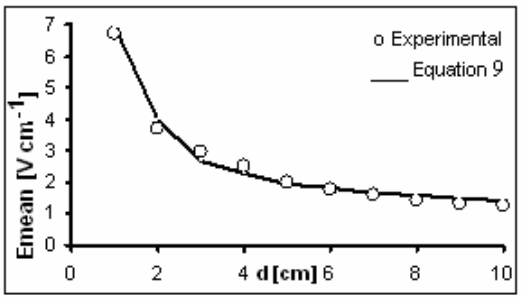

(a)

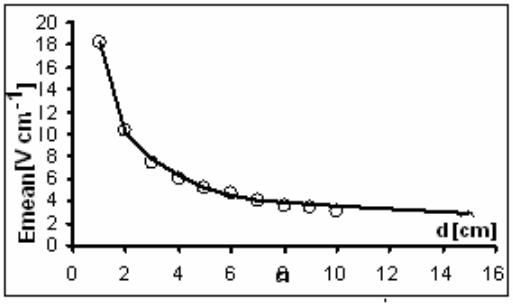

(b)

Fig. 13 E_{mean} as a function of gap spacing for two different radii at the corona inception point. (a) r=0.25mm (b) r=3.04mm

Table 4 Deviation of Value Determined by Eq. (12) as Compared to Experimental One.

Maximum & Minimum Deviations (%)			
	Rod Radius (mm)	Gap (cm)	Deviation
Max	1.07	15	19%
Min	0.5	8	0.11%

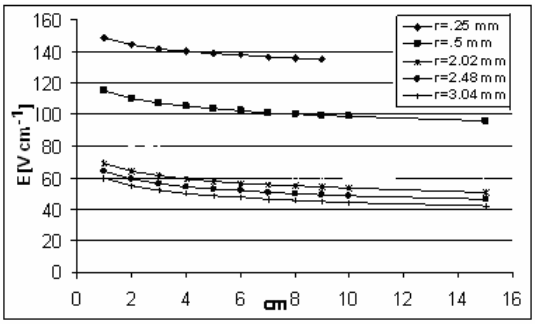

Fig. 14 Electric field at the tip of the rod, at the corona inception obtained by Equation 12 - vs. gap distance.

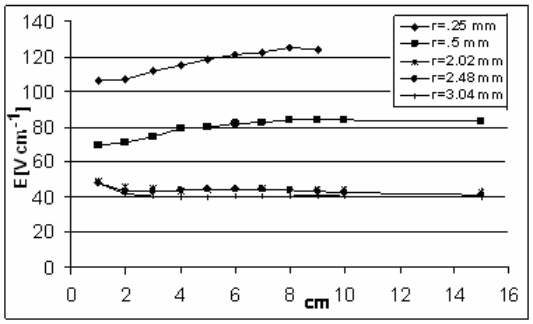

Fig. 15 Electric field at the tip of the rod, at the corona inception obtained from Equation 4 - vs. gap distance.

6 Correction Factors for Atmospheric Conditions

In order to achieve a precise temperature correction factor, the same regression method as the one used to derive E_{mean} (Eq. 7) was applied to the experimental data, thus yielding Eq. (13):

$$\frac{V_{incp}}{V_{incp(0)}} = 1.09\left(\frac{T_0}{T}\right)^{1.19} \quad ;253^{\circ}K < T < 293^{\circ}K \tag{13}$$

where V_{incp} stands for corona inception voltage at temperature T in kV (peak), $V_{incp(0)}$ is the inception voltage at the atmospheric standard condition, and T_0 is the standard atmospheric temperature, equal to 20ºC or 293ºK. That equation is plotted in Fig. 16 against the experimental results, with a maximum error of 8%.

In order to determine the correction factor due to pressure, the power regression method was applied to the $(V_{incp}/V_{incp(0)})$ and $(P_{amb}/P_{amb(0)})$ ratios of the experimental data sets, yielding Eq. (14), which is the analytical form for the calculation of V_{incp} for the standard conditions:

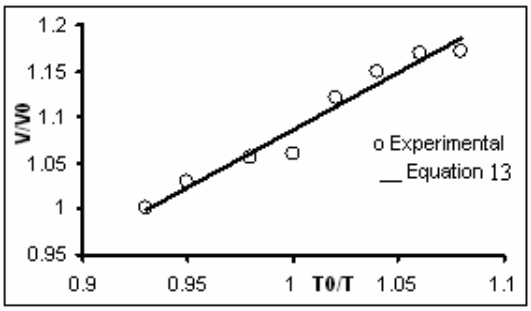

Fig. 16 Ratio of V/V_0 against ratio of T_0/T for r=1.54mm and d=7cm. T_0=273 ºK and V_0=19.5 kV (peak).

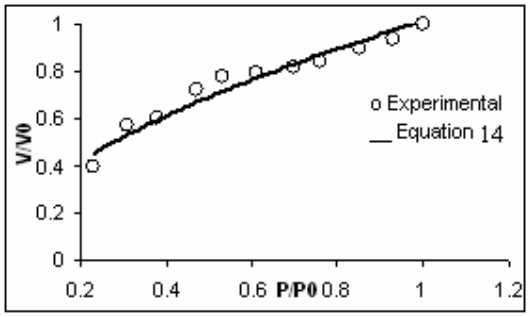

Fig. 17 Ratio of V/V_0 against ratio of P/P_0 for r=1.54mm and d=7cm. P_0=101.3kPa and V_0=19.5 kV (peak).

$$\frac{V_{incp}}{V_{incp(0)}} = \left(\frac{P_{amb}}{P_{amb(0)}}\right)^{0.5239} \quad ; 22.8kPa < P_{amb} < 101.8kPa \qquad (14)$$

where V_{incp} stands for the corona inception voltage at the ambient pressure, P_{amb}, in kV (peak), and where $V_{incp(0)}$ is the inception voltage at the atmospheric standard conditions, and $P_{amb(0)}$ is the standard atmospheric pressure, equal to 101.3 kPa. Fig. 17 shows the results obtained from Eq. (14) against the experimental ones.

7 Conclusion

Using a rod-plane electrode configuration with a radius range of 0.25mm< r <3.04mm and a gap spacing range of 1cm<d<15cm, a series of tests were carried out to measure the corona inception voltage. Computer simulation was carried out to obtain the field form factors for the electrode configuration used in the experimental setup. Also, the effects of atmospheric pressure and temperature were investigated on an electrode configuration of r=1.54mm and d=7cm with air temperature variation range of -20ºC<T_{amb}<20ºC and ambient pressure variation range of 22.8kPa<P_{amb}<101.8kPa.

Empirical equations were derived from the experimental and simulation results to calculate E_{mean}, f and E_{incp}. Moreover, correction factors for the atmospheric parameters were derived from the experimental results. The results and observations are summarized as follows:

1. Computer simulation results reveal that Eq. (13) generates very low values of E_{max} particularly for a rod-plane electrode configuration with r<1.5mm and d=4cm. The maximum error using *Coelho*'s equation occurs at r=0.25mm and d=1cm with a value of 9Vcm^{-1}, while the minimum error occurs at r=3.04mm and d=15cm with a value of 0.25Vcm^{-1}. It appears from the simulation results that *Coelho*'s equation returns fairly good results for the rod-plane configuration with r >1.54mm and d >10cm.

2. An empirical expression, Eq. (6), for calculating the field form factors for the experimental setup was derived. This equation will only be valid for 3<d/r<400 within the prescribed electrode arrangement. The results show that for this particular range, that value may reach up to 125 for (d/r)=400.

3. Based on the experimental results, Eq. (9) can be used to calculate E_{mean} for the setup electrode arrangements when the applied voltage is V_{incp}. This expression has a maximum error of 14%.

Finally, Eq. (12) was derived from both experimental and simulation results for calculating E_{incp} at the tip of the rod in a rod-plane gap. This equation provides accurate and realistic results which can replace the use of *Coelho*'s equation for the prescribed rod-plane geometry ranges.

Acknowledgment

This work was carried out within the framework of the NSERC/Hydro-Quebec/UQAC Industrial Chair on Atmospheric Icing of Power Network Equipment (CIGELE) and the Canada Research Chair on Engineering of Power Network Atmospheric Icing (INGIVRE) at Université du Québec à Chicoutimi. The authors would like to thank the CIGELE partners (Hydro-Québec, Hydro One, Réseau Transport d'Électricité (RTE) and Électricité de France (EDF), Alcan Cable, K-Line Insulators, Tyco Electronics, CQRDA and FUQAC) whose financial support made this research possible.

References

[1] Allen N. L and Hashem A. R., "The role of negative ions in the propagation of discharges across insulating surfaces", *J. Phys. D: Appl. Phys.,* Vol. 35, No. 20, pp. 2551-2557, 2002.

[2] Allen N. L., Boutlendj M. and Lightfoot H. A., "Dielectric breakdown in non-uniform field air gaps-ranges of applicability to dc voltage measurement", *IEEE Trans. on Electrical Insulation*, Vol. 28, No. 2, pp. 183-191, April 1993.

[3] Barsch J. A., Sebo S. A. and Kolico N., "Power frequency AC spark over voltage measurements of small air gaps", *IEEE Trans. On Power Delivery*, Vol. 14, No. 3, pp. 1096-1101, July 1999.

[4] Isa H., Sonoi Y. and Hayashi M., "Breakdown process of a rod-to-plane gap in atmospheric air under dc voltage stress", *IEEE Trans. On Electrical Insulation*, Vol. 26, No. 2, pp. 291-299, April 1991.

[5] Kuffel E. and Zaengl W. S., *High voltage engineering fun*damentals, Pergamon Press, Power Series 13, Peter Peregrinus Ltd., London, 1992 (ISBN 0-86341-205-X).

[6] Loeb L. B., *Electrical coronas, their basic physical mechanisms*, Univ. Calif. Press, Berkeley, 1965.

[7] Sadiku M. N. O., *Numerical techniques in electromagnetics*, 2nd edition, CRS Press 2000.

[8] Iravani M. R. and Raghuveer M. R., "Accurate field solution in the entire inter-electrode space of a rod-plane gap using optimised charge simulation", *IEEE Transaction on Electrical Insulation*, Vol. E1-17, No. 4, pp. 333-337, August 1982.

[9] Kalenderli O., Onel E. and Altay O., "Computing the corona onset and the utilisation factor of rod-plane electrode by using charge simulation method", *Electrical Insulation Conference (EIC) 2001*, pp. 453-456, Cincinnati, Ohio, USA October 16-18, 2001.

[10] Ibrahim O.E., "An expression for the electric field distribution in rod-plane gaps", *IEEE Transaction* on Electrical Insulation, Vol. 23, No. 3, pp. 493-494, June 1988.

[11] Naidu M.S., Kamaraju V., *High voltage engineering,* McGraw-Hill, New York, 1996. ISBN: 0071361081 (pbk.).

[12] General Electric Co., *Transmission Line Reference Book, 345 kV and Above*, EPRI, 1982.

[13] Coelho R. and Debeau J., "Properties of the tip-plane configuration", *Journal of Physics: Applied Physics*, Vol. 4, pp. 1266-1280, 1971.

[14] Farzaneh M., "Ice accretions on high-voltage conductors and insulators and related phenomena", *Philosophical Transactions of the Royal Society*, Vol. 358, No. 1776, pp. 2971-3005, Nov. 2000.

[15] Zhang J. and Farzaneh M., "Propagation of AC and DC arcs on ice surfaces", *Transaction on Electrical Insulation*, Vol. 147, No. 2, pp. 81-86, 2000.

[16] Fofana I. and Beroual A., "A Predictive Model of the Positive Discharge in Long Air Gaps under Pure and Oscillating Impulse Shapes", *J. Phys. D*: *Appl. Phys*., No. 30, pp. 1653-1667, 1997.

[17] Borsi H., Gockenbach E., Schroder U. and Schiller G., "Contribution to the clarification of partial discharge behaviour in insulating liquids using the Schlieren technique", *European Transactions on Electrical Power*,Vol. 1, No. 5, pp. 271-279, September 1991.

[18] Stangherlin S., Salge G. and Koenig F., *Measurement of discharges and their branching behaviour in atmospheric air*, 2002 Annual Report Conference on Electrical Insulation and Dielectric Phenomena.

[19] Qiu Y., "Simple expression of field non-uniformity factor for hemispherically capped rod-plane gaps", *IEEE Transaction on Electrical Insulation,* Vol. 21, No. 4, pp. 673-675, August 1986.

[20] Farzaneh M. and Fofana I., "Experimental study and analysis of corona discharge parameters on an ice surface", *J. Phys. D*: *Appl. Phys*., Vol. 37, pp. 721-729, 2004.

[21] Shu L., Zhao Z., Jiang X., Tian Z. and Wang J., "Effect of atmospheric pressure on discharge performance of short air-gaps at altitude of 4000 m and above", *Proc of the 7th International Conf. on Properties and Applications of Dielectric Materials*, June 1-5, Nagoya ,2003.

[22] Mikropoulos P. N. and Stassinopoulos C. A., "Atmospheric correction in rod-plane gaps up to 1 m in length", *IEE Proc.-Sci. Meas. Technol.*, 2005.

[23] IEC Publication 60060-1/1989, *High-voltage test techniques, part 1*: *General definitions and requirements*.

[24] Boutlendj M., Allen N. L., Lightfoot H. A. and Neville R. B., "Positive DC corona and spark over in short and long rod-plane gaps under variable humidity conditions", *IEE Proc.-A*, Vol. 138, No. 1, January 1991.

[25] Boutlendj M. and Allen N. L., "Assessment of air-density correction for practical electrode systems"*, Eur. Trans. Electr. Power,* Vol. 6, No. 4, pp. 267-274, July/August 1996.

[26] Javadi H. and Farzaneh M., "Measuring of corona discharge inception voltage to determine electric field over the non-homogenous electrodes in the air insulation", 19th *Int. Power System Conf.*, Tehran, 2004.

[27] Peyda A., "Numerical and experimental investigation to determine corona inception electric field, using a rod-plane configuration*", M.Sc. Dissertation*, UQAC, Canada, May 2007.

Hamid Javadi received his BSc in Electrical Engineering from Sharif University of Technology (Tehran-Iran) in 1980, his Master from UMIST (Manchester-UK) in 1986, and his PhD degree in 1994 from the Institute National Polytechnique du Toulouse (INPT) then, he joined to Electrical Engineering department of Power and Water Institute of Technology (PWIT) at Tehran as assistance professor. Following this he became associate professor in 2002. In 2004, he spent one year as invited

professor within the framework of the NSERC/Hydro-Quebec/UQAC Industrial Chair on Atmospheric Icing of Power Network Equipment (CIGELE) at university of Quebec at Chicoutimi where he continued as a postdoctoral fellow in 2005. He currently is the research deputy of Electrical engineering department of PWUT. He authored /co-authored 65 scientific publications.

Masoud Farzaneh (M' 83 - SM' 91- F'07) received his electrical engineering degree from the École Polytechnique of Iran in 1973, and a Ph.D. and a Doctorat d'État from Institut nationale polytechnique and Université Paul Sabatier, France, in 1980 and 1986, respectively. From 1980 to 1982, he was Associate Professor at Université des Sciences et de la Technologie d'Oran, Algeria. He joined Université du Québec à Chicoutimi (UQAC) in 1982 as a Guest Professor. Following this, he became a Full Professor, as well as Founder and Director of the Master's Degree Program in Engineering. Currently, he is Chair holder of the NSERC/Hydro-Quebec Industrial Chair on Atmospheric Icing (CIGELE), and Chair holder of the Canada Research Chair on Atmospheric Icing Engineering of Power Networks (INGIVRE). He is also Founder of the International Research Centre on Atmospheric Icing and Engineering of Power Networks (CENGIVRE) of which he is currently Director. He is author and co-author of close to 750 scientific publications in the domain of high voltage, outdoor insulation and atmospheric icing.

Dr Farzaneh is a Fellow of IEEE, Fellow of the Institution of Electrical Engineers (IEE), Fellow of the Engineering Institute of Canada (EIC), Charter Member of the International Society of Offshore and Polar Engineers (ISOPE) as well as member of the New York Academy of Sciences and the American Association for the Advancement of Sciences. He is currently Associate Editor of IEEE Transactions on Dielectrics and Electrical Insulation, Chairman of the IEEE DEIS Outdoor Insulation Committee, Convenor of CIGRÉ WG B2.29 on Anti- and De-Icing Systems for HV and UHV Overhead Lines as well as Chairman or member of several other working groups and task forces of IEEE and CIGRÉ dealing with atmospheric icing of HV equipment.

Arash Peyda received his B.Sc. degree in Electrical Engineering with a major in Power from Tehran Polytechnique in 1997 and M.Sc. degree in Electrical Engineering with a major in High Voltage from Université du Québec a Chicoutimi, Canada in 2007. He is a recipient of the best student paper award in ICEES in 1998, Iran and several grants and scholarships in Canada. He has worked as a Power Consultant for Moshanir Power Consultants in Iran, Electrical Installations Designer for Ausco in Australia and he is currently working as a Protection and Control Engineer for Great Lakes Power in Ontario, Canada